

# Effect of Microstructure of Nitrogen-Doped Graphene on Oxygen Reduction Activity in Fuel Cells

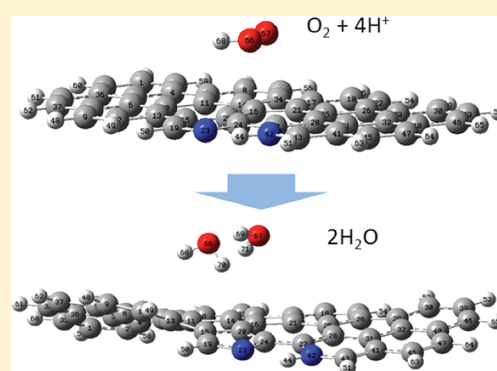
Lipeng Zhang,<sup>†</sup> Jianbing Niu,<sup>‡</sup> Liming Dai,<sup>§</sup> and Zhenhai Xia<sup>\*,‡</sup>

<sup>†</sup>Department of Mechanical Engineering, University of Akron, Akron, Ohio 44325, United States

<sup>‡</sup>Department of Materials Science and Engineering, Department of Chemistry, University of North Texas, Denton, Texas 76203, United States

<sup>§</sup>Department of Macromolecular Science and Engineering, Case Western Reserve University, 10900 Euclid Avenue, Cleveland, Ohio 44106, United States

**ABSTRACT:** The development of fuel cells as clean-energy technologies is largely limited by the prohibitive cost of the noble-metal catalysts needed for catalyzing the oxygen reduction reaction (ORR) in fuel cells. A fundamental understanding of catalyst design principle that links material structures to the catalytic activity can accelerate the search for highly active and abundant nonmetal catalysts to replace platinum. Here, we present a first-principles study of ORR on nitrogen-doped graphene in acidic environment. We demonstrate that the ORR activity primarily correlates to charge and spin densities of the graphene. The nitrogen doping and defects introduce high positive spin and/or charge densities that facilitate the ORR on graphene surface. The identified active sites are closely related to doping cluster size and dopant–defect interactions. Generally speaking, a large doping cluster size (number of N atoms >2) reduces the number of catalytic active sites per N atom. In combination with N clustering, Stone-Wales defects can strongly promote ORR. For four-electron transfer, the effective reversible potential ranges from 1.04 to 1.15 V/SHE, depending on the defects and cluster size. The catalytic properties of graphene could be optimized by introducing small N clusters in combination with material defects.



## INTRODUCTION

Molecular oxygen reduction reaction (ORR) is a dominant process in many fields, such as energy conversion (fuel cells, metal-air batteries, etc.), corrosion, or biology.<sup>1–4</sup> For fuel cells, cathodic ORR plays an essential role in producing electricity and is a major limiting factor on their performance.<sup>5,6</sup> Traditionally, platinum and its alloys<sup>7–9</sup> are used as electrocatalysts to promote the chemical reaction. However, platinum is expensive and susceptible to time-dependent drift<sup>10</sup> and CO poisoning.<sup>2</sup> These problems have been one of the major barriers in the development of fuel cells for large-scale commercial application. Thus, developing inexpensive electrocatalysts with high catalytic activity will accelerate the process of fuel cell commercialization.

Graphene and its derivatives represent a novel class of two-dimensional carbon nanomaterials. The 2D planar atomic-thick graphene exhibits better electronic properties due to its more free electron transport when compared with other forms of carbon, while many unique properties remain including excellent electronic, mechanical, and thermal properties. Previous studies have shown that graphene containing nitrogen atom has improved ORR activity, 3 times higher than platinum.<sup>11</sup> It is believed that the superior catalytic capabilities of these N-doped carbon nanomaterials are directly related to their unique nanostructure. Among the nitrogen-doped

structures, pyrrolic and pyridinic nitrogen were reported to play an important role in the enhanced ORR activity in alkaline<sup>11–14</sup> and acidic<sup>15,16</sup> solutions. Stone-Wales defects have been predicted to alter the electronic properties (band structure and density of states) of graphene,<sup>17–19</sup> and in so doing modify its chemical reactivity toward adsorbates, and likely impact its catalytic properties. Although some theoretical work has been done on ORR pathways on N-doped graphene,<sup>20–22</sup> the role of materials structures, including N distribution and defects, played in ORR, remains unclear. Understanding how microstructure influences the catalytic behavior of the graphene will guide design and optimization of the electrocatalytic electrodes and discovery of new catalysts.

In this study, we demonstrate via first-principles simulation that the ORR activities are directly correlated to material microstructure. The active catalytic sites are more likely to locate at the area with higher positive charge density and/or positive spin density. The number of dopants in cluster and Stone-Wales defects strongly affects the ORR on the N-doped graphene. This work motivates a direction for design of carbon nanostructured materials to improve their catalytic efficiency,

**Received:** November 6, 2011

**Revised:** April 10, 2012

**Published:** April 10, 2012

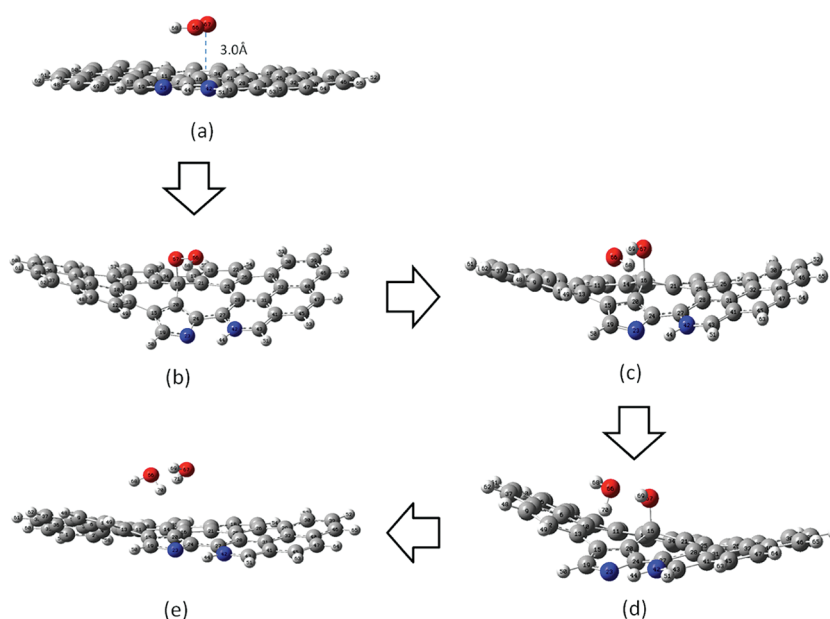


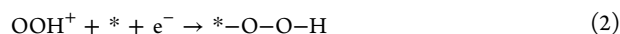
**Figure 1.** Optimized structure of each electron transformation in oxygen reduction reaction: (a) Initial position of OOH from nitrogen-doped graphene, (b) OOH adsorbs on the graphene, (c) O–O bond is broken, (d) one water molecule is generated, and (e) C–O bond is broken; the second water molecule is generated. Gray, blue, red, and small white balls represent carbon, nitrogen, oxygen, and hydrogen atoms, respectively.

and provides a theoretical framework for analysis of catalytic properties versus material structures.

## METHODS

The ORR on nitrogen-doped graphene (G) in acidic fuel cells was studied using B3LYP hybrid density functional theory (DFT) through *Gaussian 03* (revision E.01; Gaussian, Inc., Wallingford, CT, 2004). The basis set for calculation is ground state and 6-31G(d,p).<sup>23–26</sup> Nitrogen atoms were incorporated into the armchair edge of the graphene to form pyridinic or pyrrolic or mixed structures. Stone–Wales dislocations were also generated on the graphene. Stone–Wales defects are one type of important topological defects in  $sp^2$ -bonded carbon materials, playing a central role in the formation and transformation of carbon nanostructures.

We simulated the ORR processes starting with the first electron transformation, following the work on a Pt(111) by Wang et al.<sup>5</sup> Their work suggests that, in an acidic environment, a decomposition is primarily driven by the chemisorption of hydroxyl, in line with Yeager's dissociative chemisorption proposal for the first step of ORR.<sup>27</sup> A unified mechanism for the first reduction step, which combines Damjanovic's<sup>28</sup> proton participation in the first electron reduction step and Yeager's dissociative chemisorption of  $O_2$ , is summarized as follows:



or



where the asterisk represents a chemisorption site on graphene. In this step, we set OOH,  $OOH^+$  or  $O_2$  near the graphene plane at a distance of 3 Å, as schematically shown in Figure 1a. The optimized structures for OOH,  $OOH^+$  or  $O_2$  adsorption (ads) to graphene were obtained through structural optimization calculations. It is well-known that, overall, ORR can proceed by a two-step two-electron pathway with the formation of hydrogen peroxide or by a more efficient four-electron process to combine oxygen with electrons and protons directly in water. Hence, the ORR on graphene could follow either a two-electron

pathway or four-electron process, which will be examined in the simulation of subsequent electron transforming reactions.

The succeeding electron transforming reactions were simulated by continuing to add H atoms in the system. For each step, we obtained the optimized structure, and calculated the adsorption energy<sup>29</sup> (bond strength) for those molecules on the nitrogen-doped graphene. The adsorption energy is defined as the energy difference between the adsorption and the isolated systems, while the bond strength is equal to the value of the adsorption energy but with opposite sign. Here, the energy of the isolated system refers to the sum of the energies of the four-step adsorbed graphene and the individual isolated adsorbate molecules. So, negative adsorption energy indicates that the adsorbate molecule would be energetically favorable to be adducted to the surface of the nitrogen-doped graphene.

The reversible potential of each reaction step on the nitrogen-doped graphene was also calculated following the procedure described by Roques and Anderson.<sup>30</sup> For an electrochemical reaction with reactants Ox and products Red



the relationship between the Gibbs free energy for a reduction reaction in aqueous (aq) solution and the reversible potential,  $U^0$ , is<sup>30</sup>

$$U^0 = \Delta G^0/nF \quad (6)$$

where  $\Delta G^0$  is the Gibbs free energy change of eq 5,  $n$  is the number of electrons involved in the reaction, and  $F$  is the Faraday constant. In this work, the Gibbs energy change is replaced by the reaction energy,  $E_r^0$ , plus constants.<sup>30</sup> So, eq 6 becomes

$$U^0 = E_r^0/nF + U_1 + U_2 \quad (7)$$

where the first constant  $U_1$  represents  $P\Delta V$  and  $T\Delta S$  energy contributions, which depends on the solvation model used for the reactants and the products.<sup>30</sup> The second constant ( $U_2 = -4.6$  V) comes from the fact that the energy of an electron at 0 V on the electrochemical scale is  $-4.6$  eV on the physical (vacuum) scale,<sup>30</sup> which is the one in which the quantum calculations take place. Equation 7 is the reversible potential in aqueous solution. For the reaction on a catalyst surface

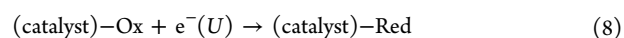


**Table 1.** Adsorption Energy Difference and Reversible Potentials of Each ORR Step on the Graphene with Two Doped Nitrogen Atoms and Two Stone-Wales Defects

reaction order	chemical reaction	adsorption energy difference $\Delta E_r$ (eV)	reversible potential $U^0$ (V/SHE) <sup>a</sup>	reversible potential $U$ (V/SHE)
1	$O_2 + H^+ + e^- \rightarrow *OOH$	1.170	-0.046	1.120
2	$*OOH + H^+ + e^- \rightarrow *OH + OH$	1.150	-0.664	0.480
3	$OH + H^+ + e^- \rightarrow H_2O$	0.0	2.813	2.813
4	$*OH + H^+ + e^- \rightarrow H_2O$	-2.320	2.813	0.493
Overall	$O_2 + 4H^+ + 4e^- \rightarrow 2H_2O$	0.00	1.229	1.228

<sup>a</sup>Ref 31.

the reversible potential  $U$  can be extrapolated from eq 7 assuming the constants  $U_1 + U_2$  unchanged

$$U = U^0 + (E_r - E_r^0)/nF \quad (9)$$

The change in reaction energy between eq 5 and eq 8,  $\Delta E_r$ , is equal to the total adsorption energy of the reactants  $E_{ads}(Ox)$ , minus the total adsorption energy of the products  $E_{ads}(Red)$ :<sup>31,32</sup>

$$\begin{aligned} \Delta E_r &= E_r - E_r^0 \\ &= E_{(ads)}[Ox] - E_{(ads)}[Red] \end{aligned} \quad (10)$$

So, the reversible potential on catalyst surface  $U$  is a function of adsorption energy and standard reversible reduction potentials  $U^0$ , for the reactions in bulk solutions:<sup>31,32</sup>

$$U = U^0 + \Delta E_r/nF \quad (11)$$

where  $U^0$  is the standard solution-phase potential. Thus, if we know the reversible potential in an aqueous solution of a redox reaction  $U^0$  (from experimental or theoretical investigations), we will be able to calculate the reversible potential on a specific catalyst surface  $U$  just by the knowledge of the adsorption energies of each species involved in the reaction.

It should be noticed that, in the ORR we study here,  $OOH^+$  and  $H^+$  exist in aqueous solution but the total adsorption energy of the chemical species are calculated using  $OOH$  and  $H$ . This is reasonable because the effect of charge has been considered by using the known reversible potential in an aqueous solution of a redox reaction  $U^0$ . The predictions are very close to the experimental results.<sup>30–32</sup> Nevertheless, care should be taken when using this method to calculate the reversible potentials. For example, the coverage rate of  $OH(ads)$  and  $OOH(ads)$  on graphene may be considered in order to get more accurate results, in particular, when comparison is made between different pathways and concerning the existence of species like  $OOH$  in solution (and not near the surface) or  $OH$  in solution.

## RESULTS AND DISCUSSION

**Catalytic Pathways of ORR on N-Doped Graphene.** We first studied catalytic pathways of graphene with two nitrogen atoms incorporated into the hexagon and the pentagon of the graphitic sheet with two combined Stone-Wales defects, as shown in Figure 1. Such structures are pyridinic and pyrrolic mixed type of nitrogen atoms in the nitrogen-doped graphene. As mentioned above, there are two possible reaction pathways in the first electron transfer: (i) intermediate molecule  $OOH^+$  adsorption and (ii) direct  $O_2$  adsorption. We first simulated the ORR processes beginning with the first electron transformation in an acidic environment, in which process an intermediate molecule  $OOH^+$  has been formed. The simulation shows that both  $OOH^+$  and  $OOH$  far from the graphene ( $\sim 3 \text{ \AA}$ ) can adsorb on the graphene at carbon atom #16, as shown Figure 1b. This result indicates that there is no energy barrier in the reaction. After adsorption, the graphene plane distorted

into “saddle shape” warped surface while the carbon atom attached to the oxygen rises out of the plane to form a tetrahedral structure.

The  $O_2$  adsorption on the N-doped graphene was simulated with the same procedure as  $OOH$  adsorption.  $O_2$  cannot adsorb on the graphene at carbon atom #16, even when the  $O_2$  molecule is put in the range of bonding formation. However,  $O_2$  can adsorb on the same site of the negatively charged graphene. The adsorbed  $O_2$  can further interact with an  $H^+$  to form an adsorbed  $OOH$ . Therefore, the surface charge promotes the adsorption of  $O_2$ . However, the  $O_2$  adsorption energy is  $-0.7 \text{ eV}$ , over 10 times smaller than that for  $OOH^+$  adsorption ( $-11.26 \text{ eV}$ ). This implies that  $OOH^+$  adsorption is a more favorable reaction in the first electron transfer.

When adding an H atom near the oxygen atom that attaches to the graphene, a bond is formed between the oxygen and the hydrogen atoms. At the same time, the O–O bond is broken, resulting in the formation of a hydroxide molecule  $OH$ , as shown in Figure 1c. During this process, the distance between the two O atoms changed from an initial value of  $1.45 \text{ \AA}$  to a value of  $2.72 \text{ \AA}$ . The dissociated  $OH$  moves away from the graphene plane, while the other dissociated  $OH$  is still bonding to the graphene. This is a typical four-electron reaction because the O–O bond breaks during the reaction.<sup>33,34</sup> After adding two more H atoms to the O atoms in the reaction system, two water molecules are formed and completely departed from the graphene (Figure 1d,e). The third and fourth electrons were then transformed in the oxygen reduction reaction. Finally, after the removal of the water molecules, the “saddle-shaped” graphene recovers to its original shape and is ready for the next reaction cycle.

The above chemical reactions, adsorption energy difference between reactants and products, standard reversible potential, and reversible potential on the catalyst surface are listed in Table 1. For each step of electron transformation, the reversible potential is positive, suggesting that the system moves to a more stable state during the reactions. So, the four-electron reaction can spontaneously take place on this nitrogen-doped graphene. Of all the reaction steps,  $OOH$  molecular adsorption on the graphene (reaction 1) is one of the most important steps for the catalytic reaction of oxygen reduction, because it determines whether a nitrogen-doped graphene electrode has catalytic activity or not. The O–O bond break in reaction 2 is another key necessary step for the four-electron reaction. The reversible potential for overall ORR is  $U_s^0 = 1.228 \text{ V(SHE)}$ , which is consistent with standard reversible potential of ORR.<sup>35,36</sup> It should be noted that, during the ORR process, carbon #16 is not the only one active site for the ORR. We



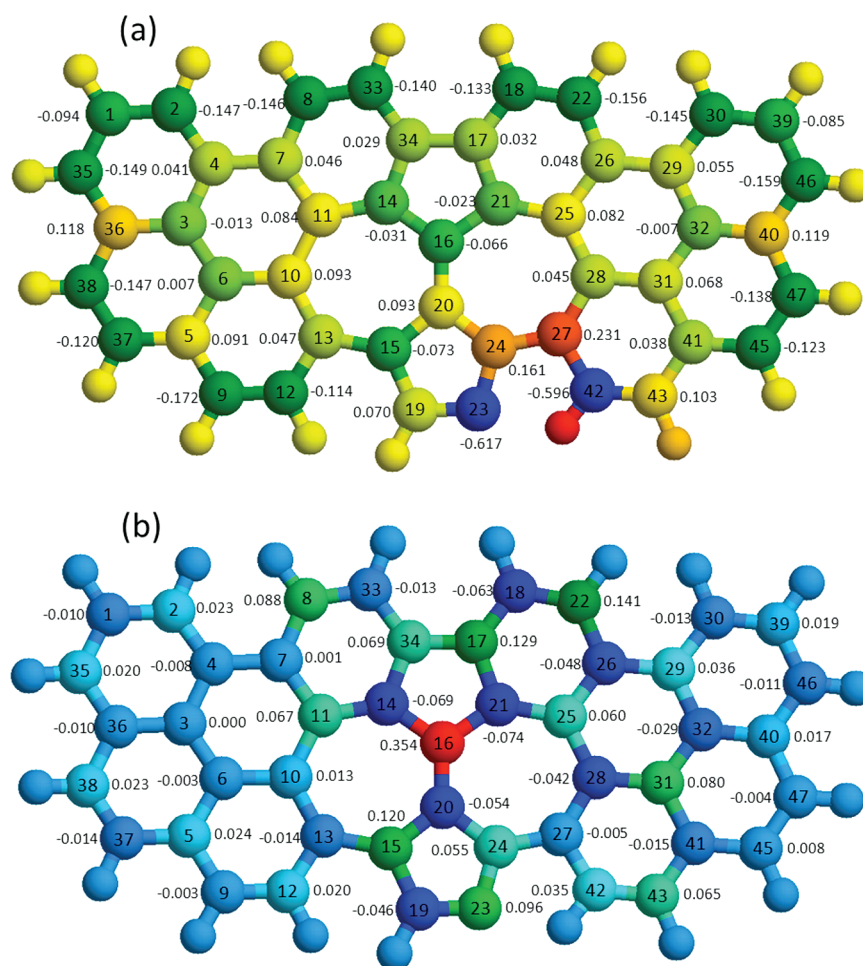


**Figure 2.** (a) Atomic charge density and (b) spin density distributions on the nitrogen-doped graphene with Stone-Wales defects. The number near each atom is the value of charge or spin density on the atom.

found that OOH molecule is also able to adsorb to carbon #27 and #24 and the succeeding reactions can occur spontaneously.

From quantum mechanics, the nitrogen doping creates an electron acceptor state in the conduction band near the Fermi level.<sup>37,38</sup> The electron-accepting ability of the nitrogen atom creates net positive charge on adjacent carbon atoms in the graphene plane, resulting in redistribution of spin density and charge density around the nitrogen atoms, which will influence the OOH adsorption and further O–O bond breakage. It was shown that the adsorption bond strengths of adsorbate radicals, H and OOH, exhibit a correlation with the spin density.<sup>29</sup> So, spin density may be regarded as a factor determining positional selectivity of radical adsorption, while charge density determines the attractive force between charged atoms. It is expected that the active catalytic sites for OOH adsorption should be those atoms with high spin density and/or high positive charge. We have calculated the spin density and charge density for a given N-doped structure. Figure 2 shows the typical spin density and charge density distributions on the nitrogen-doped graphene. For an N dopant, the atoms with high charge density are always those bonded to the nitrogen atoms, while those with high spin density are the second or third neighboring carbon atoms. Most identified active sites are those carbon atoms with high charge or spin density or high value of combination of charge and spin. For example, for the graphene with two doped nitrogen atoms and Stone-Wales

defects, carbons #27 and #24 possess the highest and second highest atomic charge density (Figure 2a) while carbon #16 has the highest spin density (Figure 2b). These atoms are the catalytic active points identified for the ORR.

As mentioned above, OOH adsorption on graphene represents one of the most important steps for ORR. The adsorption energies of OOH may be sensitive to atomic charge density and spin density of the active sites. We have calculated the charge and spin densities of active sites on several kinds of nitrogen-doped graphene structure, in which the number of doped nitrogen atoms increases from one to four in the cluster. Figure 3 shows the adsorption energy as a function of atomic charge density  $e$  and spin density  $s$ . For atomic charge density  $e = -0.087 \sim +0.085$ , and  $e = +0.205 \sim +0.263$ , the adsorption energy increases nearly linearly with increasing spin density (Figure 3a), which is consistent with the results obtained by Sidik and Anderson.<sup>29</sup> On the other hand, the adsorption energy also increases with increasing atomic charge density but with large scattering (Figure 3b). It should be noted that, for the case of no spin density, only those atoms with relatively high charge density can act as a catalytic site, but these sites with high charge density usually lead to much higher adsorption energy. Therefore, any approaches that increase the spin or charge density of carbon atoms will facilitate the ORR on graphene surface.

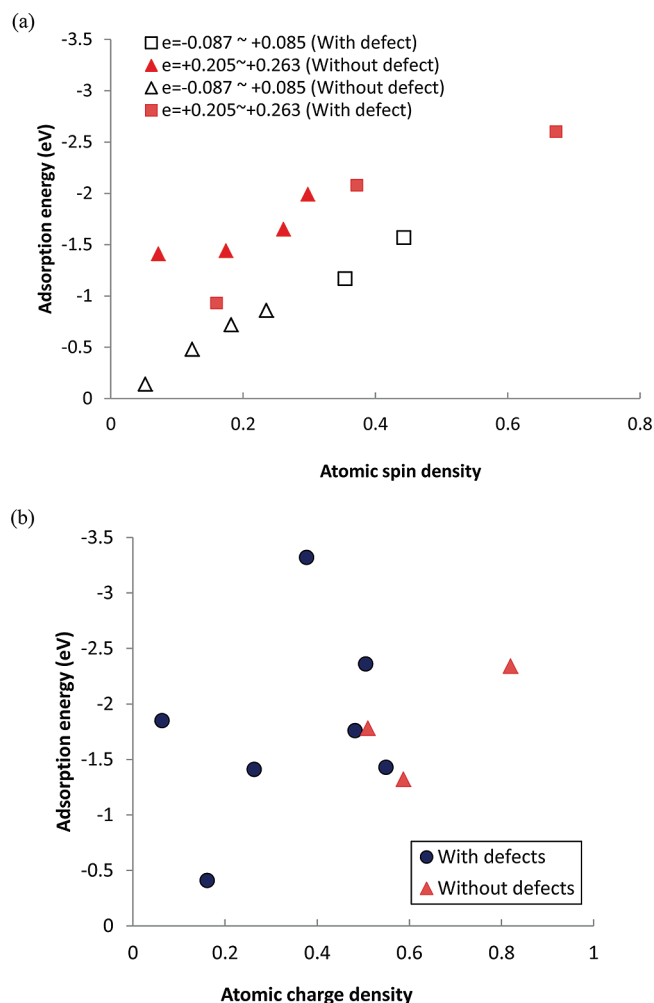


**Figure 3.** Adsorption energy of OOH on graphene as a function of (a) spin density for atomic charge  $e = -0.087 \sim +0.085$  and  $e = +0.205 \sim +0.263$  and (b) atomic charge density for  $s = -0.036 \sim +0.0072$ . The adsorption energy is calculated from reaction 15 in the absence of charge.

The above energy calculation was performed without considering the presence of charge. We have calculated the adsorption energy of  $\text{OOH}^+$  adsorbed on the graphene that carries a negative charge. As expected, the charge on graphene does influence adsorption; however, the reaction energy is closely correlated with that in the absence of charge. For example, for  $\text{OOH}^+$  adsorption reaction on the graphene (G) shown in Figure 1a



the reaction energy is  $-11.25$  eV. It consists of two elementary reactions



with reaction energies of  $1.80$  eV (graphene electron affinity) and  $-11.89$  eV ( $\text{OOH}$  ionization potential), respectively. For the same reaction without considering the charge



with a reaction energy of  $-1.16$  eV. Thus, the reaction energy of reaction 12 should be the energy sum of reactions 13–15.

Since reactions 13 and 14 compose the deionization process of  $\text{OOH}$  and graphene, their reaction energy should be constant for a given graphene structure under the standard condition. Thus, the adsorption energy calculated without considering the charge  $E_1$  is equal to that in the presence of charge  $E_2$ , plus a constant  $c$ :  $E_1 = E_2 + c$ .

As externally introduced charges may influence the charge and spin density on graphene and further ORR process, we have examined the charge and spin density distribution on N-doped graphene in the presence of an additional negative charge. It turns out that the additional charge does not influence the charge distribution on graphene (slight variation in magnitude). Thus, the additional charge does not affect the ORR mechanisms on the graphene. On the other hand, the spin density change is complicated in the presence of charges. When one additional negative charge is introduced onto the graphene, the spin density disappears. When two additional negative charges are introduced, the spin density redistributes, but the overall distribution is similar to those before the charge is introduced, i.e., there is always one carbon atom with a maximum spin density of  $\sim 0.35$ – $0.4$ , adjacent to the nitrogen atoms. In this case, the catalytic ability should remain similar even when additional charges are introduced. More work is needed to understand the radical reactions and the effect of spin density on graphene.

**Effect of Nitrogen Doping Structures and Defects on the Catalytic Behavior.** Apart from the structures with two nitrogen doping atoms, we have examined the catalytic activities of various graphene structures with a cluster of dopants and defects (Figure 4). Note that N atoms are

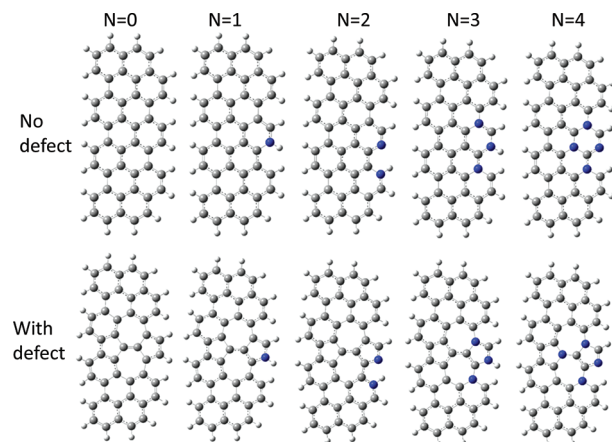


**Figure 4.** Graphene structures with a number of dopants and defects.  $N$  = the number of nitrogen dopants. Gray, blue, and small white balls represent carbon, nitrogen, and hydrogen atoms, respectively. The structures in the first row contain no defects, while the structures in the second row do.

separated by 2–3 crystal lattices ( $\sim 2$ – $3$  Å) such that there is no N–N bond in the clusters. Recent DFT calculation showed that the formation of an N–N bond in graphene is energetically unfavorable, and the probability of having two doped N atoms at neighboring sites is quite low.<sup>39</sup> More recently, scanning tunnel microscopy (STM) direct imaging on N-doped graphene revealed that most N atoms exist either isolated or in clusters in which N atoms are separated in several lattices.<sup>40</sup> We also calculated the energies of all these optimization structures of nitrogen-doped graphene with N–N bonds and

those with N atoms separated. The energy of the former is higher than that of the latter. So all the clusters generated in this study are energetically favorable.

The reaction energy and reversible potential for each reaction step of ORR on these nitrogen-doped graphene were calculated. Figure 5 shows the reversible potential for each

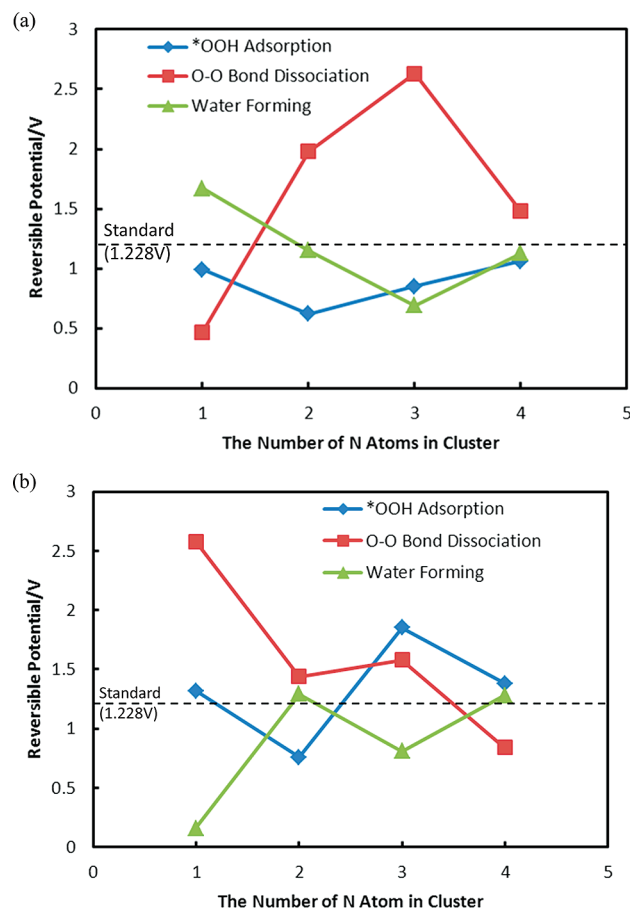


**Figure 5.** Reversible potentials of ORR versus *N* cluster size for the graphene (a) without defects and (b) with defects. Dotted lines represent standard reversible potential (1.228 V).

reaction step of ORR as a function of the number of N doping atoms. The OOH molecule cannot adsorb on graphene without N doping, indicating that the N doping is a key to graphene as an ORR catalyst. For the graphene without defects, with increasing the number of nitrogen atoms in the cluster, the reversible potential of O–O bond dissociation rapidly increases, while the potential of water formation is slightly reduced, but the potential for \*OOH adsorption does not change too much. Therefore, the N clustering can significantly promote the O–O bond dissociation reaction. For the graphene with defects, the reversible potential changes quite differently compared to N doping alone. When the size of N clusters increases, the reversible potential of O–O bond dissociation quickly reduces to a value around the standard reversible potential (1.228 V, dot lines in Figure 5), whereas the potential for water forming quickly increases to the same range. The potential for \*OOH adsorption varies slightly around the standard value. So, in the presence of defects, the N clustering makes the reversible potentials of each reaction step closer to the ideal reversible potential. Relatively equal potentials in each reaction step may increase the reaction rate in ORR.<sup>29</sup> These results suggest that

ORR occurs more easily on the nitrogen doping cluster with defects than the single nitrogen doping. Although the defects alone do not have catalytic capability, the combination of the N cluster and defects can strongly facilitate the ORR on graphene.

The N cluster and defects also influence the reaction pathway. In addition to the reaction path listed in Table 1, different reaction routes and catalytic behaviors were observed for multiple-doping graphene. The identified reaction pathways include two-electron transfer (path ① in Figure 6) and four-

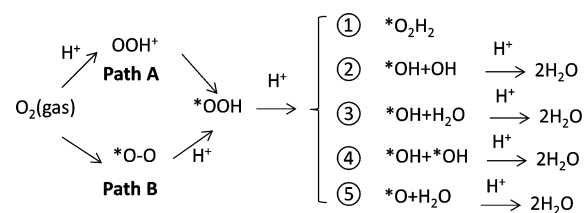


**Figure 6.** Reaction scheme of ORR on N-graphene in acidic solution, where Path A presents an intermediate OOH adsorption mechanism and Path B a direct O<sub>2</sub> adsorption mechanism, and ①–⑤ represent 5 reaction pathways after OOH adsorption.

electron transfer (paths ②–⑤). Path ① is a typical two-electron transfer reaction, while all other reaction paths identified are four-electron transfer reactions. The reversible potential for path ① is 0.685 V, which is consistent with the results from the literature.<sup>29</sup> The two-electron process usually is much less efficient than four-electron one.<sup>12</sup> For path ③, the introduction of a hydrogen results in O–O bond breaking and formation of two OH molecules. One adsorbs on the same site as the OOH on graphene, while the other combines with H that bonds to a nitrogen atom to directly form a water molecule. Finally, the adsorbed OH combines with H to form a water molecule. The overall reaction reversible potential is 1.228 V. Path ④ is similar to that listed in Table 1, but here, both OH molecules adsorb on graphene. In the last path (Path ⑤), O–O bond breaking generates an adsorbed O and a water molecule. H further reacts with the adsorbed O to form water. The overall reversible potential is also 1.228 V, which is equal to the standard reversible potential  $U^0$  of oxygen and hydrogen redox reactions. This value corresponds to the standard Gibbs energy of reaction,  $\Delta G^0 = 4.916$  eV, and is the maximum energy available to do electrical work.

The above reversible potentials were calculated under the assumption that all the Gibbs free energy is converted into electric work. However, the experimentally observed onset potential for O<sub>2</sub> reduction to water over nitrogen-doped graphene and carbon nanotube is usually much smaller than the standard reversible potential 1.228 V. This overpotential is caused by the exergonicity of OOH (ads) dissociation step.<sup>35</sup> In principle, any exergonic reaction that does not include the transfer of an electron during the course of the overall reaction will cause the overpotential, even if all of the electron transfer steps are activationless. In this study, the OOH (ads) dissociation reaction occurs on the N-doped graphene in four electron transfer ORR. For path ②, reaction 2 in Table 1 can be separated into two subreactions:  $\text{*OOH} \rightarrow \text{*O} + \text{OH}$  and  $\text{*O} + \text{e}^- + \text{H}^+ \rightarrow \text{*OH}$ . Similarly, O–O bond dissociation reaction in path ③ contains two subreactions:  $\text{*OOH} \rightarrow \text{*O} + \text{OH}$  and  $\text{*O} + \text{OH} + 2\text{e}^- + 2\text{H}^+ \rightarrow \text{*OH} + \text{H}_2\text{O}$ , while in path ④, the dissociation reaction is  $\text{*OOH} \rightarrow \text{*O} + \text{OH}$  and  $\text{*O} + \text{OH} + \text{e}^- + \text{H}^+ \rightarrow \text{*OH} + \text{*OH}$ . For path ⑤, the dissociation reaction



Table 2. Number of Active Sites and Effective Reversible Potential for Nitrogen-Doped Graphene

number of N atoms in cluster		0	1	2	3	4
No defect	The number of active sites	0	1	3	2	1
	Effective Reversible potential V/SHE	-	1.04	1.07–1.15	1.07	1.15
With defect	The number of active sites	0	1	3	2	3
	Effective Reversible potential V/SHE	-	1.04	1.15	1.07–1.15	1.15

is  $*\text{OOH} \rightarrow *O + OH$  and  $*O + OH + e^- + H^+ \rightarrow *O + H_2O$ . In the ideal case, this dissociation reaction will be energetic neutral. In the nonideal case (like the reaction on catalytic surfaces), when the reaction is exergonic, free energy  $\Delta G'$  is lost. Thus,  $\Delta G'$  is not available for electrical work and should be subtracted from  $\Delta G^0$ . The Gibbs energy available for electrical work is

$$\Delta G_w = \Delta G^0 - \Delta G' \quad (16)$$

Similar to the treatment in eq 6,  $\Delta G'$  is replaced by the reaction energy  $E_{\text{ex}}$  for the exergonic reaction. Thus, the effective reversible potential  $U_{\text{eff}}$  can be written as

$$U_{\text{eff}} = -\Delta G^0/(nF) + E_{\text{ex}}/(nF) \quad (17)$$

We calculated the lost Gibbs free energy  $\Delta G'$  of exergonic reaction ( $*\text{OOH} \rightarrow *O + OH$ ) included in paths ②–⑤, yielding 0.56, 0.63, 0.30, and 0.74 eV, respectively. So, the effective reversible potentials  $U_{\text{eff}}$  of path ①, path ③, path ④, and path ⑤ are 1.09, 1.07, 1.15, and 1.04 V, respectively.

We also found incomplete reaction paths at some active sites, mostly on the graphene with large N clusters. For example, after OOH adsorption,  $O_2 + H^+ + e^- \rightarrow *OOH$  ( $U = 2.55$  V/SHE) and O–O dissociation,  $*OOH + 2H^+ + e^- \rightarrow *OH + H_2O$ , ( $U = 1.83$  V/SHE), the reversible potential of the following steps,  $*OH + H^+ + e^- \rightarrow H_2O$  is  $-1.13$  V/SHE, which cannot occur spontaneously. In all these incomplete paths, either OOH adsorption or O–O dissociation potential or both are too high. As a result, the next reactions are suppressed.

The number of active sites and effective reversible potential against the size of N clusters are summarized in Table 2. Overall, with increasing size of the N cluster, the number of active sites per nitrogen atom first increases to a maximum value at double N cluster, and then reduces linearly. In the presence of defects, more active sites are created when N dopants exist in a cluster. This effect can be attributed to the interaction between the defect and the dopants. Considering the fact that the defects make the reversible potentials closer to the ideal value (1.228 V) (Figure 5b), if N exists in the form of clustering, a small cluster (ideally two N) combining with defects would maximize the catalytic active sites available for ORR. Interestingly, recent study shows that most N dopants exist in single N or double N cluster on single-layered graphene.<sup>40</sup>

Although it is still a challenge to experimentally realize the doping of graphene or carbon nanotubes (CNTs) with N clusters, the general trends demonstrated in this study are consistent with experimental observations. For instance, a reversible (turn-on) potential around 1 V (vs SHE) was observed for N-doped CNTs in an acidic medium.<sup>41</sup> Consistent also with the present study, the overpotential for a two-electron ORR process has been previously observed to be about half that of its four-electron counterpart catalyzed by N-doped graphene and carbon nanotubes.<sup>11,12</sup> Furthermore, our preliminary results indicate that the ORR catalytic activities

of N-doped carbon nanotubes and graphene increase with the acid-oxidation to introduce structure defects. Doping of graphene with elements (S, Cl)<sup>42</sup> of similar electronegativities as that of nitrogen could also impart the ORR activities, presumably due to the doping-induced spin redistribution.

To further examine the effect of the doping and defects on the catalytic behavior of graphene, we calculated energy separation between the highest occupied molecular orbital (HOMO) and lowest unoccupied molecular orbital (LUMO), which can be used as a simple indicator of kinetic stability. The smaller energy gap means that the state of the graphene is energetically favorable to add electrons to a high-lying LUMO, to extract electrons from a low-lying HOMO, and so to form the activated complex of any potential reaction.<sup>43</sup> The HOMO–LUMO gaps of graphene with and without defects versus the number of nitrogen atoms in cluster are shown in Figure 7. In the absence of defects, the incorporation of one or

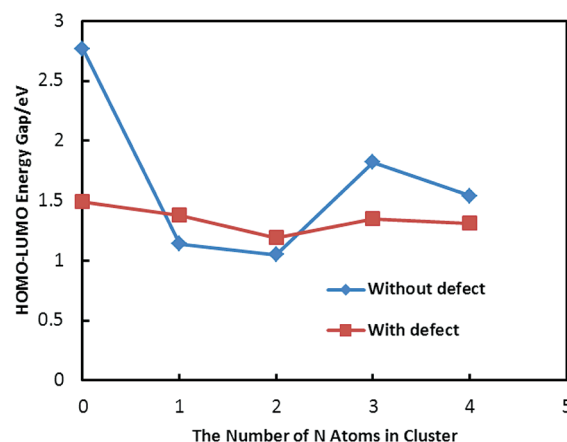


Figure 7. HOMO–LUMO energy gap as a function of the number of nitrogen-doped atoms in cluster with and without Stone-Wales defects.

two nitrogen atoms into the graphene lattice reduces the HOMO–LUMO gap by a factor of 2.3 compared to perfect graphene, but with further increasing N cluster size (3–4N), the gaps increase to a level of  $\sim 1.7$  eV from 1.1 eV. This trend is consistent with the results listed in Table 2, where the number of active sites reduces with increasing N cluster size. In the presence of Stone-Wales defects, the HOMO–LUMO energy gap is much lower than the perfect graphene. The insensitivity of the gap to the introduction of N dopants suggests that the chemical reactivity of the graphene is controlled by the defects. As a result, all the Stone-Wales defective graphene has relatively high chemical reactivity. As shown in Table 2, the number of active sites on graphene with defects is more than that on the graphene without the defects. In addition to increasing the number of active sites, defects can promote some catalytic reactions, i.e., the adsorption and O–O bond breaking reactions (Figure 5). However, in the case of a large N cluster, the combination of N cluster and defects can sometimes overpromotes these reactions with a consequence of

blocking the following reactions (i.e., water formation). As discussed above, the presence of N dopants generated active sites that have high adsorption energy (e.g., OH on graphene). However, the bonds may be too strong to break in the following reactions. Consequently, the following catalytic reactions cannot occur spontaneously. Thus, to optimize the catalytic performance, materials structures should be controlled to have small N doping clusters in combination with material defects.

## CONCLUSIONS

The DFT method was used to study the effect of nitrogen-doping and Stone-Wales defects on ORR in fuel cells. Simulation results show that dopant-induced redistribution of spin density and charge density on the graphene strongly affect the formation of the intermediate molecules in ORR, including OOH, or O<sub>2</sub> adsorption, O–O bond breaking, and water formation. With an increasing number of nitrogen dopants from one to four in the cluster, the number of active sites per doping atom reaches a maximum at  $N = 2$  and then reduces, indicating that the catalytic ability of nitrogen in a larger cluster is weaker than that of single nitrogen or a small cluster in terms of the number of catalytic sites available. The defects enhance the catalytic capability of the graphene by changing the HOMO–LUMO energy gap and reaction pathways. For four-electron transfer, the predicted effective reversible potential for N-doped graphene is in the range of 1.04–1.15 V/SHE with an average value of 1.10 V/SHE, which is consistent with the experimental results. Engineering materials structures can promote catalytic capability of graphene by introducing small N clusters in combination with materials defects.

## AUTHOR INFORMATION

### Corresponding Author

\*E-mail: Zhenhai.xia@unt.edu, Tel: 940-369-5805, Fax: 940-565-4824.

### Notes

The authors declare no competing financial interest.

## ACKNOWLEDGMENTS

The authors acknowledge the support from NSF (CMMI-1000768, and CMMI-1212259) and AFOSR MURI (FA9550-12-1-0037).

## REFERENCES

- (1) Steele, B. C. H.; Heinzel, A. Materials for fuel-cell technologies. *Nature* **2011**, *414*, 345.
- (2) Winther-Jensen, B.; Winther-Jensen, O.; Forsyth, M. High rates of oxygen reduction over a vapor phase-polymerized PEDOT electrode. *Science* **2008**, *321*, 671.
- (3) Khelashvili, G.; Behrens, S.; Vetter, C.; Hinsch, A.; Kern, R.; Skupien, K.; Dinjus, E.; Bonnemann, H. Catalytic platinum layers for dye solar cells: A comparative study. *Thin Solid Films* **2006**, *511*, 342.
- (4) Goux, A.; Pauporté, T.; Lincot, D. Oxygen reduction reaction on electrodeposited zinc oxide electrodes in KCl solution at 70 °C. *Electrochim. Acta* **2006**, *51*, 3168.
- (5) Wang, Y.; Balbuena, P. B. Ab initio molecular dynamics simulations of the oxygen reduction reaction on a Pt(111) surface in the presence of hydrated hydronium (H<sub>3</sub>O)<sup>+</sup>(H<sub>2</sub>O)<sub>2</sub>: Direct or series pathway? *J. Phys. Chem. B* **2005**, *109*, 14896.
- (6) Basu, S.; Ed. *Recent Trends in Fuel Cell Science and Technology*; Springer: New York, 2007.
- (7) Che, G.; Lakshmi, B. B.; Fisher, E. R.; Martin, C. R. Carbon nanotube membranes for electrochemical energy storage and production. *Nature* **1998**, *393*, 346.
- (8) Gong, K.; Yu, P.; Su, L.; Xiong, S.; Mao, L. Polymer-assisted synthesis of manganese dioxide/carbon nanotube nanocomposite with excellent electrocatalytic activity toward reduction of oxygen. *J. Phys. Chem. C* **2007**, *111*, 1882.
- (9) Kongkanand, A.; Kuwabata, S.; Girishkumar, G.; Kamat, P. Single-wall carbon nanotubes supported platinum nanoparticles with improved electrocatalytic activity for oxygen reduction reaction. *Langmuir* **2006**, *22*, 2392.
- (10) Collman, J. P.; Devaraj, N. K.; Decreau, R. A.; Yang, Y. A cytochrome c oxidase model catalyzes oxygen to water reduction under rate-limiting electron flux. *Science* **2007**, *315*, 1565.
- (11) Qu, L.; Liu, Y.; Baek, J. B.; Dai, L. Nitrogen-doped graphene as efficient metal-free electrocatalyst for oxygen reduction in fuel cell. *ACS Nano* **2010**, *4*, 1321.
- (12) Gong, K.; Du, F.; Xia, Z.; Dustock, M.; Dai, L. Nitrogen-doped carbon nanotube arrays with high electrocatalytic activity for oxygen reduction. *Science* **2009**, *323*.
- (13) Luo, Z.; Lim, S.; Tian, Z.; Shang, J.; Lai, L.; MacDonald, B. Pyridinic N doped graphene: synthesis, electronic structure, and electrocatalytic property. *J. Mater. Chem.* **2011**, *21*, 8038.
- (14) Shao, Y.; Zhang, S.; Engelhard, M. H.; Li, G.; Shao, G.; Wang, Y. Nitrogen-doped graphene and its electrochemical applications. *J. Mater. Chem.* **2010**, *20*, 7491.
- (15) Lee, K.; Lee, J.; Ahn, B.; Woo, S. Electrochemical oxygen reduction on nitrogen doped graphene sheets in acid media. *Electrochem. Commun.* **2010**, *12*, 1052.
- (16) Wang, P.; Wang, Z.; Jia, L.; Xiao, Z. Origin of the catalytic activity of graphite nitride for the electrochemical reduction of oxygen: geometric factors vs. electronic factors. *Phys. Chem. Chem. Phys.* **2009**, *11*, 2730.
- (17) Meyer, J. C.; Kisielowski, C.; Erni, R.; Rossell, M. D.; Crommie, M. F.; Zettl, A. Direct imaging of lattice atoms and topological defects in graphene membranes. *Nano Lett.* **2008**, *8*, 3582.
- (18) Boukhvalov, D. W.; Katsnelson, M. I. Chemical functionalization of graphene with defects. *Nano Lett.* **2008**, *8*, 4373.
- (19) Banhart, F.; Kotakoski, J.; Krashenninnikov, A. V. Structural defects in graphene. *ACS Nano* **2011**, *5*, 26.
- (20) Zhang, L.; Xia, Z. Mechanism of oxygen reduction reaction on nitrogen-doped graphene for fuel cells. *J. Phys. Chem. C* **2011**, *115*, 11170.
- (21) Kim, H.; Lee, K.; Woo, S. I.; Jung, Y. On the mechanism of enhanced oxygen reduction reaction in nitrogen-doped graphene nanoribbons. *Phys. Chem. Chem. Phys.* **2011**, *13*, 17505.
- (22) Yu, L.; Pan, X.; Gao, X.; Hu, P.; Bao, X. Oxygen reduction reaction mechanism on nitrogen-doped graphene: A density functional theory study. *J. Catal.* **2011**, *282*, 183.
- (23) Ditchfield, R.; Hehre, W. J.; Pople, J. A. Self-consistent molecular-orbital methods. IX. an extended Gaussian-type basis for molecular-orbital studies of organic molecules. *J. Chem. Phys.* **1971**, *54*, 724.
- (24) Hehre, W. J.; Ditchfield, R.; Pople, J. A. Self-consistent molecular orbital methods. XII. further extensions of Gaussian-type basis sets for use in molecular orbital studies of organic molecules. *J. Chem. Phys.* **1972**, *56*, 2257.
- (25) Hariharan, P. C.; Pople, J. A. The influence of polarization functions on molecular orbital hydrogenation energies. *Theor. Chem. Acc.* **1973**, *28*, 213.
- (26) Franci, M. M.; Pietro, W. J.; Hehre, W. J.; Binkley, J. S.; DeFrees, D. J.; Pople, J. A.; Gordon, M. S. Self-consistent molecular orbital methods. XXIII. a polarization type basis set for second row elements. *J. Chem. Phys.* **1982**, *77*, 3654.
- (27) Yeager, E. Electrocatalysts for O<sub>2</sub> reduction. *Electrochim. Acta* **1984**, *29*, 1527.
- (28) Sepa, D. B.; Vojnovic, M. V.; Vracar, L. M.; Damjanovic, A. Different views regarding the kinetics and mechanisms of oxygen reduction at Pt and Pd electrodes. *Electrochim. Acta* **1987**, *32*, 129.



- (29) Sidik, R. A.; Anderson, A. B. O<sub>2</sub> reduction on graphite and nitrogen-doped graphite: experiment and theory. *J. Phys. Chem. B* **2006**, *110*, 1787.
- (30) Roques, J.; Anderson, A. B. Pt<sub>3</sub>Cr(111) alloy effect on the reversible potential of OOH (ads) formation from O<sub>2</sub> (ads) relative to Pt (111)<sup>1</sup>. *J. Fuel Cell Sci. Technol.* **2005**, *2*, 86.
- (31) Kurak, K. A.; Anderson, A. B. Nitrogen-treated graphite and oxygen electroreduction on pyridinic edge sites. *J. Phys. Chem. C* **2009**, *113*, 6730.
- (32) Roques, J.; Anderson, A. B. Electrode potential-dependent stages in OH<sub>ads</sub> formation on the Pt<sub>3</sub>Cr alloy (111) surface. *J. Electrochem. Soc.* **2004**, *151*, E340.
- (33) Walch, S.; Dhanda, A.; Aryanpour, M.; Pitsch, H. Mechanism of molecular oxygen reduction at the cathode of a PEM fuel cell: Non-electrochemical reactions on catalytic Pt particles. *J. Phys. Chem. C* **2008**, *112*, 8464.
- (34) Chen, R. R.; Li, H. X.; Chu, D.; Wang, G. F. Unraveling oxygen reduction reaction mechanisms on carbon-supported Fe-Phthalocyanine and Co-Phthalocyanine catalysts in alkaline solutions. *J. Phys. Chem. C* **2009**, *113*, 20689.
- (35) Feng, T.; Anderson, A. B. Effective reversible potential, energy loss, and overpotential on platinum fuel cell cathodes. *J. Phys. Chem. C* **2011**, *115*, 4076.
- (36) Ruvinskiy, P. S.; Bonnefont, A.; Pham-Huu, C.; Savinova, E. R. Using ordered carbon nanomaterials for shedding light on the mechanism of the cathodic oxygen reduction reaction. *Langmuir* **2011**, *27*, 9018.
- (37) Webster, S.; Maultzsch, J.; Thomsen, C.; Liu, J.; Czerw, R.; Terrones, M.; Adar, F.; John, C.; Whitley, A.; Carroll, D. L. Raman characterization of nitrogen doped multiwalled carbon nanotubes. *Mater. Res. Soc.* **2003** 772, M7.8.1.
- (38) Soin, N.; Roy, S.; Hazra, K. S.; Misra, D. S.; Lim, T. H.; Hetherington, C. J.; McLaughlin, J. A. Enhanced and stable field emission from in situ nitrogen-doped few-layered graphene nanoflakes. *J. Phys. Chem. C* **2011**, *115*, 5366.
- (39) Huang, S.; Terakura, K. First-principles calculation of the electronic properties of graphene clusters doped with nitrogen and boron: Analysis of catalytic activity for the oxygen reduction reaction. *Phys. Rev. B* **2009**, *80*, 235410.
- (40) Zhao, L.; He, R.; Rim, K. T.; Schiros, T.; Kim, K. S.; Zhou, H.; Gutierrez, C.; Chockalingam, S. P.; Arguello, C. J.; Palova, L.; Nordlund, D.; Hybertsen, M. S.; Reichman, D. R.; Heinz, T. F.; Kim, H. P.; Pinczuk, A.; Flynn, G. W.; Pasupathy, A. N. Visualizing individual nitrogen dopants in monolayer graphene. *Science* **2011**, *333*, 999.
- (41) Xiong, W.; Du, F.; Liu, Y.; Perez, A.; Supp, M., Jr.; Ramakrishnan, T. S.; Dai, L.; Jiang, L. 3-D carbon nanotube structures used as high performance catalyst for oxygen reduction reaction. *J. Am. Chem. Soc.* **2010**, *132*, 15839.
- (42) Dai, J.; Yuan, J.; Giannozzi, P. Gas adsorption on graphene doped with B, N, Al, and S: A theoretical study. *Appl. Phys. Lett.* **2009**, *95*, 232105.
- (43) Aihara, J. Reduced HOMO-LUMO gap as an index of kinetic stability for polycyclic aromatic hydrocarbons. *J. Phys. Chem. A* **1999**, *103*, 7487.